Rev. LatinAm. Metal. Mat.

Artículo Regular

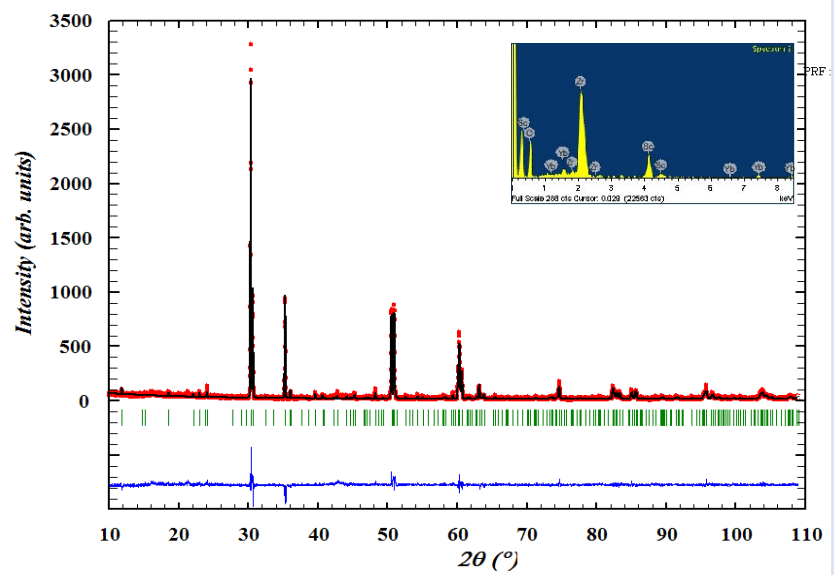
www.rlmm.org

THE OXIDATION BEHAVIOR OF YTTERBIUM SCANDIUM ZIRCONIUM NITRIDES UNDER NONISOTHERMAL CONDITIONS

Neil J. Martinez[1], Eberhard Schweda[2], Aurora Molina[1], Francis Cordero[3],

1: Materials Science Department. Simon Bolivar University. Edif. MEM. Valle de Sartenejas, 1080 Baruta, Venezuela.
2: Institut für Anorganische Chemie der Universität Tübingen, Auf der Morgenstelle 18 , 72076 Tübingen, Germany.
3: ISS International SpA, Via Magna Grecia 117, 00183 Rome, Italy.

**e-mail: neilmartinez@usb.ve*



ABSTRACT

Ytterbium codoped scandium stabilized zirconia, $Zr_{0,60}Sc_{0,175}Yb_{0,225}O_{1,8}$ was synthesized and nitrided for 48 h under an ammonia atmosphere. The compound obtained was nominally $Zr_{0,60}Sc_{0,175}Yb_{0,225}O_{0,0627}N_{1,157}$ with a red color and a cation deficient rocksalt structure. Its stability and reoxidation behavior was studied by differential thermal analysis (DTA) and thermogravimetric analysis (TG) under non-isothermal conditions. For evaluation of the experimental data, the Coats Redfern method [1] was used and revealed that the decomposition of the nitride to form ytterbium scandium zirconium oxide is diffusion controlled. The activation energy for the decomposition process was found to be 506 KJ/mol compared to 103 KJ/mol for ZrN [2]. The results indicate that scandium-zirconium-nitrides co-doped with lanthanide metals undergo a reduction in O^{2-} and N^{3-} mobility in the crystal and consequently a delay in the reoxidation process.

Keywords: Thermal stability of nitrides, non-isothermal TG/DTA/DDTA, ytterbium, scandium zirconium.

REACCIÓN DE OXIDACIÓN DE NITRUROS DE CIRCONIA CON ESCANDIO E ITERBIO BAJO CONDICIONES NO ISOTÉRMICAS

RESUMEN

La circonia estabilizada con escandio e iterbio, $Zr_{0,60}Sc_{0,175}Yb_{0,225}O_{1,8}$ fue sintetizada y sometida a nitruración por 48 horas bajo una atmosfera de NH_3. La composición nominal obtenida fue $Zr_{0,60}Sc_{0,175}Yb_{0,225}O_{0,0627}N_{1,157}$, la cual presentó una coloración rojiza y una estructura tipo sal de roca con deficiencia cationica. Su estabilidad y comportamiento en procesos de reoxidación fue estudiada por análisis térmico diferencial y termogravimétricos bajo condiciones no-isotérmicas. Los datos experimentales fueron evaluados utilizando el método de Coats Redfern method [1] que reveló que el proceso de descomposición de este material es controlado por difusión. La energía de activación para el proceso de descomposición fue de 506 KJ/mol comparado con 103 KJ/mol para ZrN [2]. Estos resultados indican que los nitruros de escandio-circonia co-dopados con metales del grupo lantánido, presentan una reducida movilidad de las especies O^{2-} and N^{3-} en el cristal y en consecuencia una menor velocidad de reoxidación.

Palabras clave: Estabilidad térmica de nitridos, TG/DTA/DDTA no isotérmico, zirconio.

Recibido: 19-07-2013 ; **Revisado:** 12-09-2013
Aceptado: 25-10-2013 ; **Publicado:** 11-19-2013

pISSN: 0255-6952 | eISSN: 2244-7113
Rev. LatinAm. Metal. Mat. 2014; **34** (2): 275-281

1. INTRODUCTION

Zirconium nitrides have lately gained considerable interest because of their properties such as super hardness, electronic conductivity and improved thermal and mechanical behavior. These nitrides are widely used as wear-resisting coatings, structural materials and diffusion barriers in advanced device semiconductor technologies [3].

Among these metal nitrides, ZrN and scandium stabilized zirconium nitride (ScSZN), are potential materials for future applications in microelectronics such as thin film resistors and barrier ceramics. These nitride materials are best prepared by a nitridation using ammonia at around 1473 K. During this process the corresponding oxynitrides and finally nitrides are formed.

The oxynitrides were found to crystallize sometimes with a fluorite related superstructure but the nitrides crystallize with a cation deficient rock salt structure. These latter materials then have quite reasonable electronic and ionic conductivities [4,5,6]. An understanding of the reoxidation behavior on air as well as the thermal stability of a nitride like YbScSZN is important, if such materials are used for coatings.

From the literature, only a few models for the reaction path of such reoxidation reactions are known. In the case of the reoxidation of Si_3N_4 several processes are said to be involved and it is assumed that the rate constant might be limited by oxygen diffusion, nitrogen diffusion by both or additionally by a reaction including an interface containing N_2 bubbles [7,8]. Such gas bubbles of N_2 can form only if the permeability or diffusion rate of N_2 through the preformed oxide layer is substantially lower than that of oxygen. The time required to initiate the formation of gas bubbles would depend on the non-stoichiometry of the starting compound. Raman spectroscopy proved such N_2 species to be present in ScSZN [5]. Another point is the rough surface morphology after reoxidation. Electron microscopy reveals a cratered surface,for the ScSZN material after reoxidation, which also might be evidence for a gas bubble release [9].

We studied and compared the reoxidation reaction for ScSZN and YbScSZN. The reoxidation reaction is believed to involve four steps. An oxygen diffusion through the crystal surface, the transfer of nitrogen atoms towards the surface; the production of N_2 molecules along with the reduction of O_2 and finally the desorption of N_2.

The activation energy for nitrogen diffusion in Sc doped zirconia was found to be 1,8 eV (174 kJ/mol) while for oxygen was 1eV (96 kJ/mol) [9]. This means that oxygen diffusion starts first. The presence of an additional lanthanide ion in scandia stabilized zirconia will reduce the ionic and electronic conductivity in such compounds.

2. EXPERIMENTAL PART

A microcrystalline powder of $Zr_{0.60}Sc_{0.175}Yb_{0.225}O_{1.8}$ (YbScSZ) with a molar ratio Zr/Sc 48/14 containing 3 mol% of Yb_2O_3 was synthesized by the polymer complex method [10]. This compound was characterized using X-ray diffraction (XRD), scanning electron microscopy (SEM) and energy dispersive X-ray analysis (EDX), and then reacted for 2d at 1473 K with ammonia to generate $Zr_{0,60}Sc_{0,175}Yb_{0,225}O_{0,0627}N_{1,157}$ with a red color and a cation deficient sodium chloride structure.

The different phases were identified by XRD within a scan range between 10° - 110° (XRD; Siemens D5000 θ/θ, CuK (λ = 1.5418 Å).

Thermogravimetric and differential thermal analysis (TG/DTA) experiments were carried out using a Netzsch STA 449F3 Thermoanalyser. Scans were measured in an atmosphere of air at different heating rates (2, 5 and 10 K/min).

3. RESULTS AND DISCUSSION

Rietveld refinement of the X-ray diffractogram of $Zr_{0,60}Sc_{0,175}Yb_{0,225}O_{1,8}$ established $R\bar{3}$ as space group for the fluorite related supercell with lattice constants a = 9.5399(7) Å and c = 17.4770(8) Å, as well as a random distribution of the cations Zr/Sc/Yb. After nitridation, the diffractogram of the corresponding nitride, $Zr_{0,60}Sc_{0,175}Yb_{0,225}O_{0,0627}N_{1,157}$ exhibited a cation deficient rock salt structure $Fm\ \bar{3}m$ with a cell parameter a = 4.5431(1) Å. These cells were larger compared to $Zr_{10}Sc_4O_{26}$ [5] ($R\bar{3}$: a = 9.4941(1) and c = 17.4252(1) Å) due to the difference of ionic radius between Sc^{3+} (87 pm) and Yb^{3+} (98 pm) [11]. The results of SEM/EDX analysis for $Zr_{0.60}Sc_{0.175}Yb_{0.225}O_{1.8}$ proved Yb and Sc as dopant cations (Yb_{M5} = 1.526 keV and Sc_K = 4.493 keV).

©2014 Universidad Simón Bolívar

3.1 TG and DTA results

The sample weight increased continuously up to 1100 K during the reoxidation reaction. The mayor weight increase (90%) occurred between 850 and 1010 K. Analyses of the DTA curves showed that the increase took place in two exothermic steps for YbScZN while only one exothermic step was found for ScZN.

The reduction process of oxygen:

$$O_2 + 4\ e^- \rightarrow 2\ O^{2-}$$

is endothermic and requires the dissociation energy of O_2 (498 kJ/mol) as well as the electron affinity (704 kJ/mol) to sum 1202 kJ/mol.

The oxidation process of N^{3-}:

$$2N^{3-} \rightarrow N_2 + 6\ e^-$$

is exothermic and calculated from the association energy (-945 kJ/mol) and the negative electron affinity ($N^{3-} \rightarrow N$ -2300 kJ/mol) to be -3245 kJ/mol.

So this redox reaction:

$$4N^{3-} + 3O_2 \rightarrow 6O^{2-} + 2N_2$$

will produce at the end one strong exothermic signal in the DTA measurements.

However, if N_2 bubbles are formed at an interface between the nitride and an O_2 saturated reoxidized surface layer, the release of dinitrogen might be delayed. The dissolution of N_2 gas bubbles then will release the surface energies of the bubbles resulting in a second exothermic peak in the DTA measurements.

Fig. 1 shows the TG/DTA data (heating rate 2K/min) for the reoxidation of ScSZN and it can be observed a strong exothermic signal at 838 K. In this case, both the reoxidation and the N_2 release occurs simultaneously because nitrogen diffusion is not hindered and an interface not formed. This is supposed to be different in YbScSZN. While Zr^{4+} and Sc^{3+} (84 pm, 87 pm) have similar ionic radio. The replacement of Zr^{4+} or Sc^{3+} by Yb^{3+} (98 pm) [11] will lower the ionic mobility of N^{3-} and O^{2-} as well as the diffusion of N_2 and O_2.

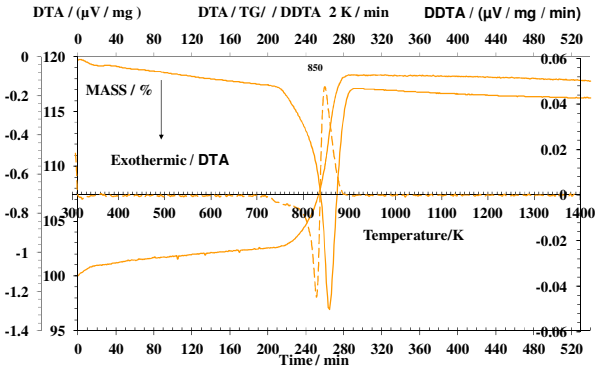


Figure 1. TG/DTA/DDTA curves of ScZN at heating rate of 2 K/min.

Figs. 2-4 show the TG/DTA/DDTA curves for the reoxidation of YbScSZN between 320 – 1200 K at different heating rates. In order to compare the results in each run, a sample of 65 mg of YbScSZN was used. At every heating rate the reoxidation reaction starts between 800 and 850 K. Contrary to the results for ScSZN (fig. 1), two different exothermic processes are clearly observed. This might be due to remarkable slower dinitrogen diffusion as a result of the formation of N_2 bubbles at the interface.

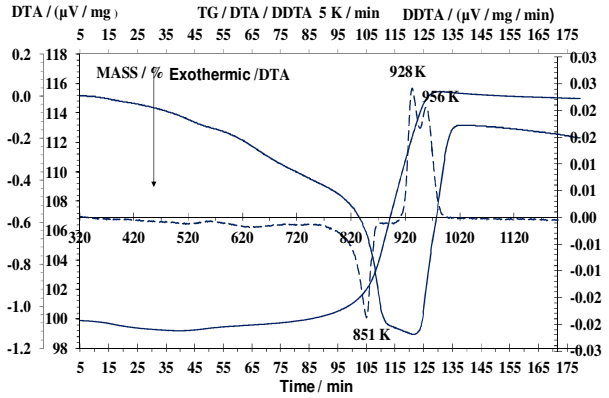


Figure 2. TG/DTA/DDTA curves of YbScZN at heating rate of 2 K/min.

For the heating rate of 2 K/min (fig. 2) the complete oxidation lasts 45 min and occurs between 835 - 920 K. For 5 K/min the time is 23 min and arises between 870 - 930 K while for a heating rate of 10 K/min the overall reaction time is 20 min and it takes place between 851 - 1057 K. This means the higher the heating rate the more separated are the two exothermic peaks. In addition, while more N_2 bubbles are evolved, the interface become thicker, consequently the second exothermic peak appears

©2014 Universidad Simón Bolívar

stronger. The complete O_2 uptake and the redox reaction occur at higher heating rates in a shorter time and a longer temperature interval (851-1057 K) and the N_2 release occurs at higher temperature with higher intensity. A deconvolution of the three different DTA-curves gives the results showed in table 1.

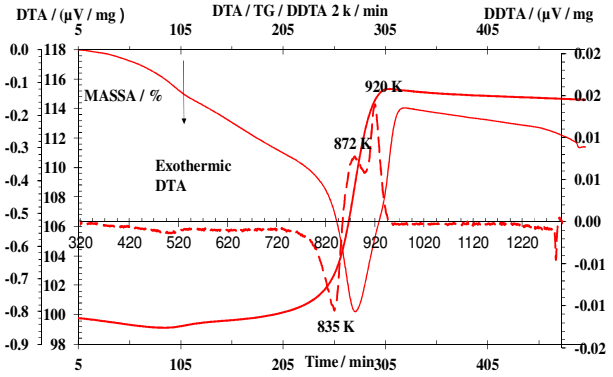


Figure 3. TG/DTA/DDTA curves for YbScZN at heating rate of 5 K/min.

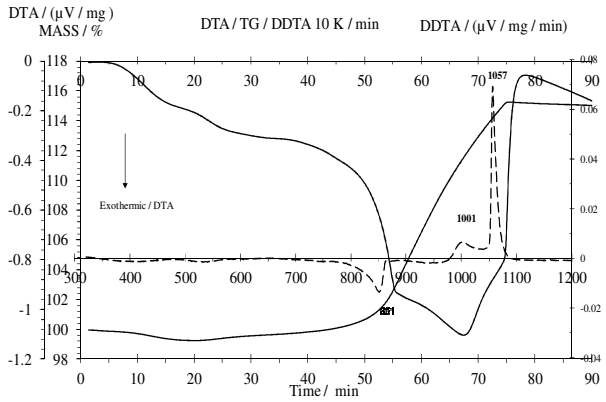


Figure 4. TG/DTA/DDTA curves for YbScZN at heating rate of 10 K/min.

At lower heating rates, the temperature interval for the complete reoxidation is only between 835 - 920 K consistent with a similar diffusion of O_2 and N_2 and therefore a small interface formation.

Finally, this reoxidation was investigated using a time and temperature dependent X-ray diffraction study and the result observed was a simple transformation from a rock salt related structure to a fluorite related structure.

Table 1. Data of the two exothermic peaks after deconvolution for the DTA curve

Heating rate *K/min*	Redox reaction Curve maximum at Temperature K	Redox reaction Curve Area Intensity	N_2-release Curve maximum Temperature K	N_2-release Curve Area Intensity
2	*580.8*	*116.5*	*629.9*	*4.8*
5	*589.8*	*193.8*	*647.3*	*92.3*
10	*598.1*	*510.4*	*730.5*	*349.8*

3.2 Crystallization, mechanism and activation energy

The original mass loss versus temperature (TG) curves obtained at constant heating rates were transformed into the degree of conversion (α) versus temperature by $(\alpha) = [m_o\text{-}m_t]/ [m_o\text{-}m_t]$, where m_t represents the mass of the sample at arbitrary time t (or temperature T), whereas m_o and m_f are the mass of the sample at the beginning and at the end of the process, respectively (fig. 5).

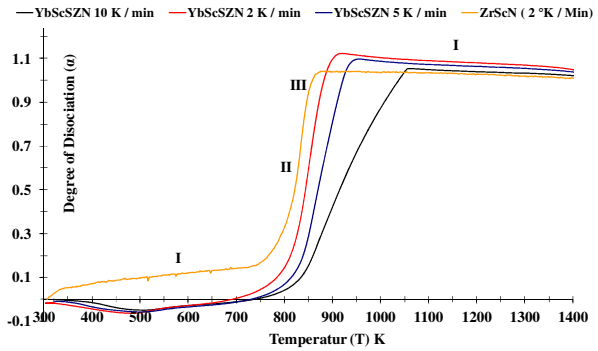


Figure 5. Crystallization α versus temperature for different heating rates (ZrScZN and YbScZN).

According to Gualtieri et al. [12] the rate of a kinetically controlled process can be expressed as:

$$\frac{d\alpha}{dt} = k\, f(\alpha) \text{ or in the integral form } g(\alpha) = kt \qquad (1)$$

Where α is the conversion factor, k the rate constant with respect to time t, f(α) is the kinetic model function which depends on the reactions mechanism and g(α) is the integral of 1/ f(α).

A non isothermal experiment takes place under a constant temperature increase. T_0 is the temperature at the beginning of the reaction and b the rate of temperature increase. The temperature at a time t is

then given by:

$$T = bt + T_0 \quad (2)$$

In order to extract kinetic data from these non-isothermal measurements, it was employed the method developed by Coats and Redfern [1]. It is based on the equation

$$ln\ g(\alpha) = \alpha\ ln\ T = ln\left[\frac{AR}{Eb}\right] - \frac{E}{RT} \quad (3)$$

Parameters A and E are determined using several expressions reported in table 2.

On the other hand, the method proposed by Kennedy and Clark [13] is given by:

$\frac{b*g(\alpha)}{(T-T_0)} = Ae^{\frac{-E}{RT}}$ Taking the logarithm of both sides of this equation gives:

$$ln\left[\frac{b*g(\alpha)}{(T-T_0)}\right] = \ln(A) - \frac{E}{RT} \quad (5)$$

Plotting the left hand side of this equation against 1/T should give a straight line with gradient –E/RT and an intercept of ln (A). Expressions for g(α) are in the Table 2.

Table 2. Different expressions for g($\boldsymbol{\alpha}$) according to different kinetic models.

Kinetic model	g(α)
John Mehl Avrami	$\left[-ln(1-\alpha)^{1/n}\right]$
Phase boundary controlled reaction (contracting area)	$\left[1-(1-\alpha)^{1/2}\right]$
Phase boundary controlled reaction (contracting volume)	$\left[1-(1-\alpha)^{1/3}\right]$
ne dimensional diffusion	$O[(\alpha)^2]$
Two dimensional diffusion (Bidimensional particles shape)	$(1-\alpha)[ln(1-\alpha)+\alpha]$
Three dimensional diffusion (Tridimensional particles shape) Jander Equation	$\left[1-(1-\alpha)^{1/3}\right]^2$
Three dimensional diffusion (Tridimensional particles shape) Ginstling-Brounshtein	$\left[1-(2\alpha/3)-(1-\alpha)^{2/3}\right]$

In this context, figure 6 shows the reoxidation behavior of $Zr_{0,60}Sc_{0,175}Yb_{0,225}O_{0,0627}N_{1,157}$ as a plot of g(α) versus 1/T for three different heating rates namely 2, 5 and 10 K/min, under dry air and normal atmospheric pressure. The curve is interpreted in four steps.

In the initial and final stage, the oxidation proceeds approximately linear with time, in a temperature range 300 to 500 K and above 1200 K. The linear behavior below 500 K might be expressed by

$$g(\alpha) = K_1 t \quad (4)$$

where K_1 is the linear rate constant and t the reaction time. In the temperature range 300 - 500 K the cation deficient nitride with NaCl structure is still present. In step II (temperature range 600 - 700 K) the oxidation process will slow down whereas in step III (above 700 K) oxidation will proceed faster. These steps can be described using the Ginstling-Brounstein equation [14]

$$g(\alpha) = [1-[(2/3)*(1-\alpha)]-[(1-\alpha)^{(2/3)}] = Kj_1 * t \quad (5)$$

where Kj_1 is the diffusion-controlled rate constant. In the step II, the degree of oxidation is up to 90% and is characteristic of an autocatalytic reaction behavior. Step III can be related to a diffusion controlled mechanism and it is attributed to the crystallization of the doped zirconium oxide.

$$g(\alpha) = \alpha^2 = K_{j2} * t \quad (6)$$

where K_{j2} is the diffusion-controlled rate constant in one dimension.

Fig. 6 shows the curves fitting using the equations of Coats and Redfern [1], Kennedy and Clark [3] and equations for the three dimensional diffusion mechanism from Ginstling-Brounstein [14] between 700 and 1000 K. For the three heating rates (2, 5 and 10 K/min), it was observed an excellent linear correlation.

The autocatalytic reaction proceeds up to 980 K with a 90 % weight increase. Throughout this process, the cell volume decreases, molecular nitrogen is lost and the oxynitride is formed. Simultaneously, it is produced a diffusion barrier for dinitrogen, consisting of oxide and oxynitride.

©2014 Universidad Simón Bolívar

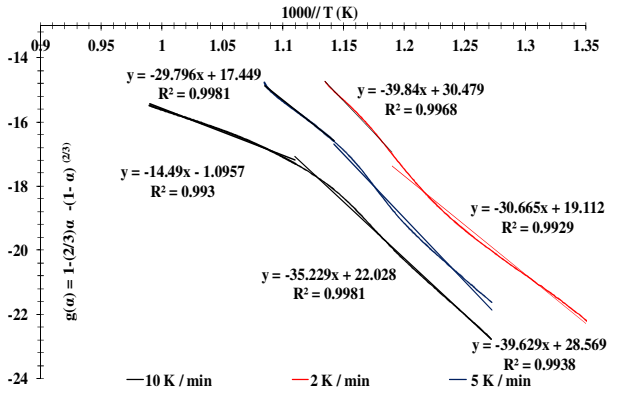


Figure 6. g (α) = [1- [(2/3)*(1-α)] – [(1-α) $^{(2/3)}$] versus 1/T fitting plots at different heating rates for the YbScSZN.

The autocatalytic process may originate from interfacial differences between the educt and the product phase. Nevertheless, the N_2 gas developed during reaction and the formation of gas bubbles play a major role in the reactions mechanism. Fig. 7 shows g(α) versus 1000/T /K for the completion of the oxidation reaction with the formation of the fluorite structure using the $g(\alpha) = (\alpha)^2$ expression for an one dimensional diffusion-controlled mechanism. From the slope of these lines, the activation energies were calculated.

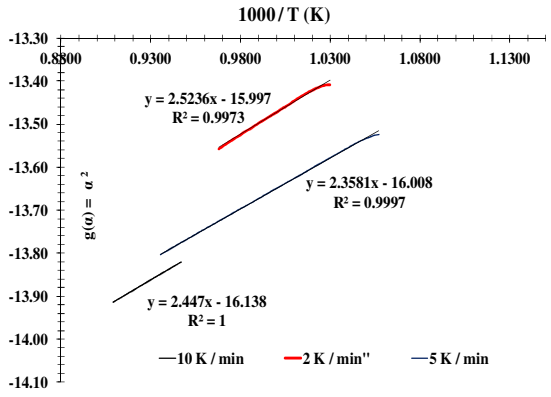


Figure 7. g (α) = α^2 versus 1/T fitting plots at different heating rates for the YbScSZN.

4. CONCLUSIONS

The transformation of YbScSZN to a crystalline oxide phase was studied using TG/DTA experiments, under non-isothermal conditions in order to extract kinetic data. The activation energy E_a = 506 KJ/mol was determined using the Coats Redfern equation and different reaction mechanisms. The best fitting for this oxidation process was achieved using the expressions g(α) corresponding to the one dimensional and three dimensional diffusion controlled mechanisms.

$$g(\alpha) = [\alpha)^2] \quad (6)$$

$$g(\alpha) = [1 - [(2/3)*(1-\alpha)] - [(1-\alpha)^{(2/3)}] = Kj_1 * t \quad (5)$$

This study suggests that the oxidation kinetics follow two different paths: oxygen diffusion and reaction with nitrogen followed by a slow evolution of molecular nitrogen. The present work shows that the oxidation of the nitride is a very complex diffusion controlled process.

5. ACKNOWLEDGEMENTS

We would like to thank Dr. Jochen Glaser (Universität Tübingen) for the thermoanalytical measurements. The financial support for this work was provided by the Simon Bolivar University (USB), the German Academic Exchange Service (DAAD), Institut für Anorganische Chemie der Eberhard Karls Universität Tübingen, and the National Fund of Science and Technology (FONACIT) from Venezuela.

6. REFERENCES

[1]. A. W. Coats, J. P. Redfern, Nature, 201, 68-69 (1964).

[2]. Y. Ikuma, A. Shoji, Advanced Materials 93'I, A: 277 (1994).

[3]. L. E. Toth., Transition Metal Carbides and Nitrides, Academic Press. New York, 1971.

[4]. N. J. Martinez Meta, E. Schweda. J. Solid State Chem., 179, 1486-1489 (2006).

[5]. N. J. Martinez Meta, E. Schweda, H. Boysen, A. Haug, T. Chassé, M. Hoelzel, Z. Anorg. Allg. Chem., 633, 790-794 (2007).

[6]. N. J. Martinez Meta, Dissertation Universität Tübingen, (2005).

[7]. B. A. Galanov, S. M. Ivanov, E. V. Kartuzov, V. V. Kartuzov, K.G. Nickel,Y.G. Gogotsi, Computational Materials Science, 21, 79-81 (2001)

[8]. K. L. Luthra, J.Am.Ceram.Soc 74, 1095-1103 (1991).

[9]. M. Lerch et al., Progress in Solid State Chem. 37, 81-131 (2009).

©2014 Universidad Simón Bolívar

[10]. D. Chen, E. Jordan, M. Gell, J. Mater. Sci, 42, 5576-5580 (2007).

[11]. R. D. Shannon, C. T. Prewitt, Acta Cryst., B25, 925-946 (1969).

[12]. A. F. Gualtieri, M. Gemmi, M. Dapiaggi, American Mineralogist, 88, 1560-1574 (2003).

[13]. J. A Kennedy, S. M. Clark, Thermochimica Acta, 307, 27-35 (1997).

[14]. A. M. Ginstling, B. I. Brounshtein, J. Appl. Chem. 23, (1950) 1327

©2014 Universidad Simón Bolívar